Supplementary Information for "Storage of 1650 modes of single photons at telecom wavelength"

Shi-Hai Wei[1], Bo Jing[1,†], Xue-Ying Zhang[1], Jin-Yu Liao[1], Hao Li[4], Li-Xing You[4], Zhen Wang[4], You Wang[1,3], Guang-Wei Deng[1,2,6], Hai-Zhi Song[1,3], Daniel Oblak[5,‡], Guang-Can Guo[1,2,6], Qiang Zhou[1,2,6,*]

[1] *Institute of Fundamental and Frontier Sciences & School of Optoelectronic Science and Engineering, University of Electronic Science and Technology of China, Chengdu 610054, P. R. China*

[2] *CAS Key Laboratory of Quantum Information, University of Science and Technology of China, Hefei 230026, P. R. China*

[3] *Southwest Institute of Technical Physics, Chengdu 610041, P. R. China*

[4] *Shanghai Institute of Microsystem and Information Technology, Chinese Academy of Sciences, Shanghai 200050, P. R. China*

[5] *Institute for Quantum Science and Technology, and Department of Physics & Astronomy, University of Calgary, 2500 University Dr. NW, Calgary, Alberta T2N 1N4, Canada*

[6] *Hefei National Laboratory, Hefei 230088, P. R. China*

*Correspondence and requests for materials should be addressed to BJ (email: † bjing@uestc.edu.cn), DO (email: ‡ doblak@ucalgary.ca), or QZ (email: * zhouqiang@uestc.edu.cn).*

Note 1: Preparation of quantum memory with five spectral channels

Due to the inhomogeneous broadening in erbium doped silica fibre (EDF) up to THz, EDF is usually utilized to prepare broadband quantum memory[1–3] and can in principle support the storage of ps-width photonic wavepackets. In this section, we present the preparation of AFCs with five spectral channels in EDF. First, the light from a continuous-wave laser (CW-laser) operating at 1531.88 nm is modulated into an optical frequency comb by cascading a phase modulator (PM) and an intensity modulator (IM)[4], at which IM is used to improve spectral flatness of the generated optical frequency comb[5]. The 15 GHz microwave signal is divided into two parts. One is sent directly to the PM, and the other is sent to the IM with a phase shifter connected, resulting in an optical frequency comb with a frequency spacing of 15 GHz, as shown in Fig.S. 1. The prepared optical frequency comb is sent to another PM to generate frequency chirping light on each comb. The modulated signal is composed of a series of sine waves with frequencies from 0 to 5 GHz. The ±1st order frequency-shifted light generated with PM has the same intensity. Therefore, by adding 0 – 5 GHz modulation signals to the PM, the frequency shift of the light ranges from -5 GHz to 5 GHz. In this way, we prepare five AFCs in the EDF with frequency chirping 10 GHz bandwidth for each channel.

In our experiment, we prepare five AFCs at the central wavelengths of 1532.11 nm, 1532.00 nm, 1531.88 nm, 1531.76 nm and 1531.65 nm, respectively. A typical example of five AFCs is shown in Fig.S. 2.

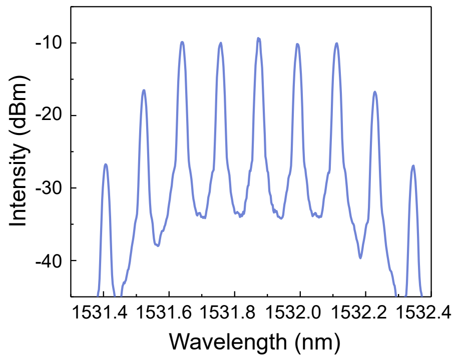

Fig.S. 1: **Optical frequency comb.** The central wavelengths of five combs with same intensity are 1532.11 nm, 1532.00 nm, 1531.88 nm, 1531.76 nm, 1531.65 nm, respectively.

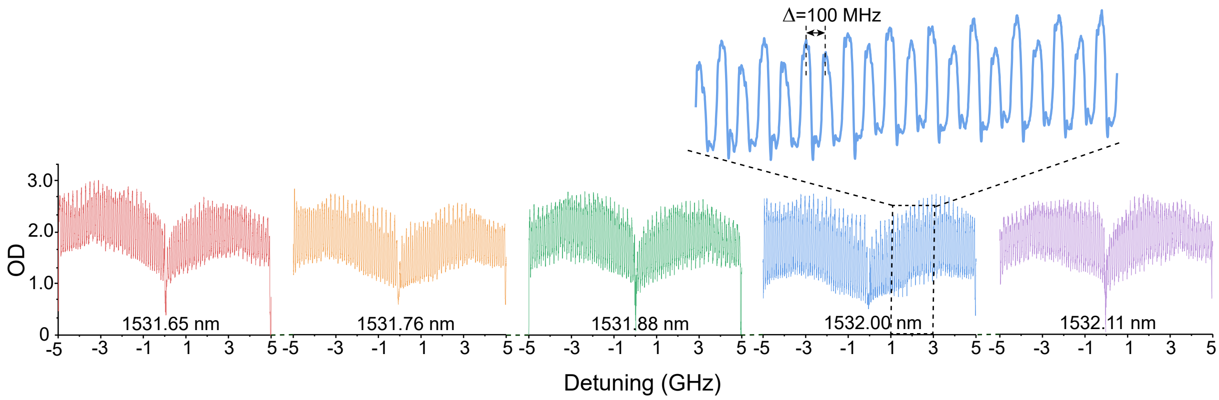

Fig.S. 2: **Typical AFCs with five spectral channels.** A typical example of AFCs with five spectral channels prepared by utilizing optical frequency comb and frequency chirping method. The bandwidth of each AFC is 10 GHz, and the spacing of adjacent AFCs is 5 GHz. In total, the available bandwidth for quantum memory is 50 GHz. Inset: Details for a 2-GHz-wide section of the AFC is shown, where the comb spacing Δ is 100 MHz. OD: Optical Depth.

Note 2: Heralded single photon source

In this section, we present properties of the heralded single photon source at telecom wavelength corresponding to different AFC spectral channels. The experimental setup is shown in Fig.S. 3. The scheme for generating correlated photon-pairs is cascaded second-harmonic generation (SHG) and spontaneous parametric down conversion (SPDC) processes in a single periodically poled lithium niobate (PPLN) waveguide[6–10] (the main parameters of the PPLN see Table S. I). The light from a narrow linewidth continuous-wave laser operating at 1540.60 nm is modulated into light pulses with a repetition rate of 1 MHz by an intensity modulator (IM) and sent into the PPLN module, resulting in correlated photon-pairs with a bandwidth of ∼60 nm. Erbium doped fibre amplifier (EDFA) and variable optical attenuator (VOA) are utilized to adjust the optical power of pump light, and polarization controller (PC) and polarizing beam splitter (PBS) are used to adjust the polarization of pump light. Dense wavelength division multiplexers (DWDMs) are

TABLE S. I: Main parameters of PPLN module.

Type of waveguide	RPE waveguide
Length of waveguide	50 mm
Poled period	19 μm
SHG normalized conversion efficiency	336.07%/W
Length of pigtail	20 cm
Input coupling efficiency of PPLN waveguide	55.51%
Output coupling efficiency of PPLN waveguide	77.89%

utilized to select signal photons (1531.88 nm) and idler photons (1549.32 nm) with a bandwidth of 100 GHz. The generated correlated photon-pairs are then sent directly to the detection system. In the measurement system, correlated photon-pairs with a bandwidth of ∼6 GHz corresponding to five channels of quantum memory are filtered out by adjusting the temperatures of two tunable fibre Bragg gratings (FBGs). The central wavelengths of signal photons corresponding to channels 1 to 5 are 1532.11 nm, 1532.00 nm, 1531.88 nm, 1531.76 nm, and 1531.65 nm, respectively. Correspondingly, the central wavelengths of idler photons are 1549.08 nm, 1549.20 nm, 1549.32 nm, 1549.44 nm, and 1549.56 nm. Finally, the selected correlated photon-pairs are detected by two superconducting nanowire single photon detectors (SNSPDs). Circulators (Cirs) are utilized to collect the reflected photons from FBGs.

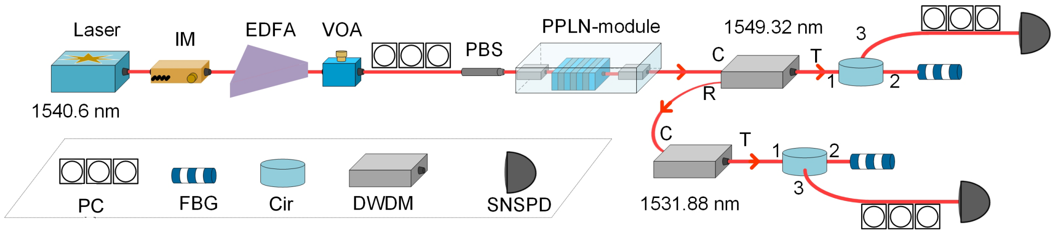

Fig.S. 3: **Experimental setup for heralded single photon source at telecom wavelength.** IM: intensity modulator, EDFA: erbium doped fibre amplifier, VOA: variable optical attenuator, PC: polarization controller, PBS: polarizing beam splitter, PPLN: periodically poled lithium niobate, DWDM: dense wavelength division multiplexer, Cir: circulator, FBG: fibre Bragg grating, SNSPD: superconducting nanowire single photon detector.

We measure the photons counting rate of correlated photon-pairs corresponding to different spectral channels under different power of pump light. Fig.S. 4(a) shows the photons counting rate of a typical correlated photon-pairs corresponding to channel 2 with different pump powers. The blue circles and red squares represent idler photons and signal photons, respectively. Here, the counting rates of signal photons and idler photons fit well with the quadratic polynomial curves. The measured counting rate of idler photons is slightly higher than signal photons. This is mainly owning to the difference in transmission efficiency and bandwidth of the filters. The total transmission loss of idler photons is 3.9 dB, including the loss of DWDM, PC, FBG, etc., while the loss of signal photons is 5.5 dB. The bandwidth of the FBG with the central wavelength of 1549.32 nm (1531.88 nm) is ∼0.06 nm (0.05 nm). Fig.S. 4(b) shows the coincidence counting of idler photons and signal photons with different pump powers. Then we measure the cross-correlation function ($g^{(2)}_{s,i}(0)$) of photon-pairs corresponding to different channels of quantum memory

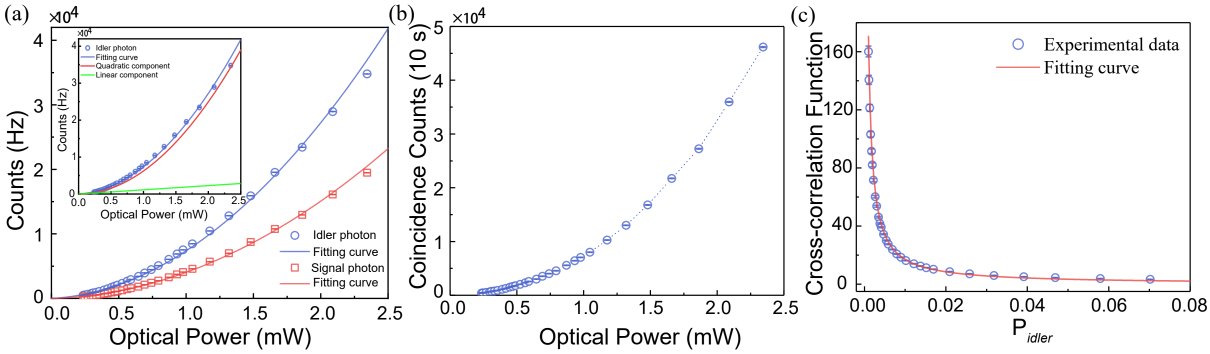

Fig.S. 4: **Measured results of correlated photon-pairs related to channel 2.** (a) Photons counting rate of signal photons and idler photons versus pump power. Inset: Idler photon-counting rate (blue circle) versus pump power. The blue solid line is the quadratic polynomial fitting curve of the photon-counting rate with the quadratic and linear parts shown as the red and green curves, respectively. The quadratic and linear components are corresponding to the contributions of generated photon-pairs and noise photons. (b) Coincidences counting rate between signal photons and idler photons versus pump power. (c) Cross-correlation function ($g^{(2)}_{s,i}(0)$) of correlated photon-pairs versus P_{idler}. All error bars are calculated by standard deviations of counts which obey Poisson distribution.

under different generation probabilities of idler photons. Fig.S. 4(c) shows $g^{(2)}_{s,i}(0)$ for typical correlated photon-pairs corresponding to channel 2 of the quantum memory with different generation probabilities of idler photons (P_{idler}). The measured $g^{(2)}_{s,i}(0)$ fits well with an inversely proportional curve. Considering that the output coupling efficiency of the PPLN module is 71.65%, the total transmission efficiency is 40.74%, and the detection efficiency of SNSPD is 60%, the measured efficiency of idler photons is 17.51%. For a measured P_{idler} of 0.62%, the intrinsic generation probability of idler photons in the waveguide is 3.54%, which results in a measured $g^{(2)}_{s,i}(0)$ of 27.53±0.18. Detailed values corresponding to each channel are shown in Table S. II.

TABLE S. II: Values of $g^{(2)}_{s,i}(0)$ for correlated photon-pairs corresponding to different channels.

Channel[a]	Signal photon (nm)[b]	Idler photon (nm)[c]	$g^{(2)}_{s,i}(0)$
1	1532.11	1549.08	25.64 ± 0.19
2	1532.00	1549.20	27.53 ± 0.18
3	1531.88	1549.32	27.91 ± 0.18
4	1531.76	1549.44	28.38 ± 0.18
5	1531.65	1549.56	28.62 ± 0.19

[a]Correlated photon-pairs corresponding to different channels of quantum memory.
[b]Central wavelengths of signal photons corresponding to different channels.
[c]Central wavelengths of idler photons corresponding to different channels.

Note 3: Performance of the five-channel quantum memories

In this section, we first take channel 2 as an example to illustrate the storage performance. Fig.S. 5(a) shows the system storage efficiency, defined as the ratio of the count rate of recalled heralded photons to that of the input heralded photons, for a typical channel of quantum memory (channel 2) versus storage time. At small storage time (< 100 ns), a slight oscillation of the storage efficiency is visible. This may be due to a quantum beat generated by the interaction of the Er^{3+} with other surrounding ions (such as the co-doped Al^{3+})[11,12]. For longer storage time, the decay is exponential with decay constant of 48 ns. We attribute this to the decoherence effects of Er^{3+} and the imperfect preparation of AFCs[1]. Fig.S. 5(b) shows $g_{s,i}^{(2)}(0)$ after storage as a function of storage time for channel 2. Unlike the efficiency, the cross-correlation function $g_{s,i}^{(2)}(0)$ remains almost constant at a level above 25 even at the maximum storage time of 230 ns. First and foremost, this shows that non-classical properties of the correlated photon-pairs are preserved in the memory and, in addition, that even at the largest storage time the signal-to-noise ratio (SNR) of the system is high enough (> 730) that the noise does not degrade the cross-correlation function. (see note 4 for more details on the role of SNR in determining $g_{s,i}^{(2)}(0)$ in our quantum memory). The cross-correlation function after storage versus storage time for all five-channel quantum memories are shown in Table S. III.

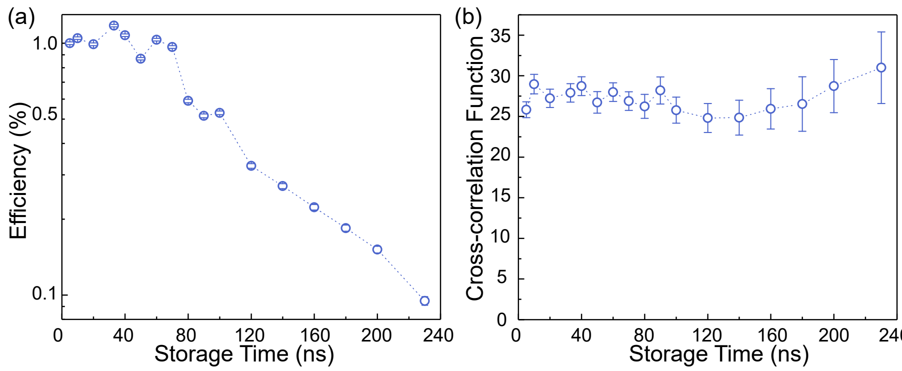

Fig.S. 5: **Performance of multi-channel quantum memory.** (a) A typical example (channel 2) for system storage efficiency as a function of storage time. The comb tooth spacing are prepared ranging from 200 to 4.35 MHz, which determines the storage time from 5 to 230 ns. (b) A typical example (channel 2) for cross-correlation function after storage as a function of storage time. The measurement time for each point is 1000 s. All error bars are calculated by standard deviations of counts which obey Poisson distribution.

Note 4: Contribution of SNR to $g_{s,i}^{(2)}(0)$

This section we present the influence of SNR of quantum memory on quantum correlation of correlated photon-pairs, where the SNR is defined as the ratio of coincidence of idler-recalled photons to idler-noise photons. The measured 3-fold coincidence detecting probability p_{si} of trigger signal, signal and idler photons, and the 2-fold coincidence detecting probability p_s (p_i) of trigger signal and signal (idler) photons are expressed as

$$\begin{aligned} p_s &= \eta_c \eta_s + \eta_n, \\ p_i &= \eta_c \eta_i + \eta_n, \\ p_{si} &= \eta_c \eta_s \eta_i + p_s p_i, \end{aligned} \tag{1}$$

TABLE S. III: Performance of each channel of quantum memory.

Storage time	Channel 1	Channel 2	Channel 3	Channel 4	Channel 5
0 ns	25.64±0.19	27.53±0.18	27.91±0.18	28.38±0.18	28.62±0.19
5 ns	25.89±1.38	25.82±0.97	26.69±1.49	26.10±1.06	25.23±1.12
10 ns	26.13±1.45	28.97±1.20	26.81±1.49	26.10±1.05	27.07±1.15
20 ns	25.97±1.49	27.23±1.13	26.48±1.50	27.35±1.05	25.26±1.15
33 ns	26.10±1.37	27.90±1.13	25.38±1.31	27.12±1.11	25.26±0.93
40 ns	26.13±1.37	28.73±1.16	26.32±1.26	28.36±1.46	25.29±0.92
50 ns	26.95±1.48	26.72±1.32	26.85±1.59	26.95±1.23	22.99±1.11
60 ns	27.05±1.53	27.99±1.15	26.95±1.54	26.01±1.00	25.49±0.91
70 ns	25.01±1.54	26.89±1.14	25.02±1.43	25.39±1.25	26.08±1.03
80 ns	25.64±1.78	26.24±1.48	26.21±1.81	25.54±1.44	24.64±1.19
90 ns	25.65±1.80	28.19±1.67	25.65±1.79	27.35±1.57	24.97±1.28
100 ns	26.08±1.90	25.77±1.60	24.48±1.92	27.01±1.69	25.85±1.36
120 ns	27.12±2.31	24.80±1.78	27.05±2.33	28.70±1.69	22.95±1.50
140 ns	25.00±2.31	24.85±2.15	23.97±2.36	24.46±2.25	27.60±1.93
160 ns	23.99±2.76	25.93±2.43	22.36±2.63	28.26±2.78	23.71±1.78
180 ns	24.99±3.25	26.53±3.35	24.89±3.51	26.53±3.25	23.45±2.34
200 ns	25.46±3.17	28.75±3.37	20.76±3.27	26.05±3.17	25.57±2.60
230 ns	26.22±4.32	31.00±4.41	26.22±4.32	26.59±3.81	22.09±3.34

where η_c is the internal generation probability of correlated photon-pairs in the waveguide, η_s is the overall measured efficiency of recalled signal photons including transmission, storage, collection and detection efficiency, η_i is the overall measured efficiency of idler photons, and η_n is the detected probability of noise photons in each experimental trial, respectively. The $p_s \cdot p_i$ gives a good estimation for the accidental coincidences of uncorrelated background[13]. Combining Eq. (1) with Eq. (2) in main text, $g_{s,i}^{(2)}(0)$ can be calculated as

$$g_{s,i}^{(2)}(0) = \frac{p_{si}}{p_s \cdot p_i} = \frac{\eta_c \eta_s \eta_i}{(\eta_c \eta_s + \eta_n) \cdot (\eta_c \eta_i + \eta_n)} + 1. \tag{2}$$

During the experiment, η_s is the only considered efficiency that will decrease with increasing storage time, and detection of idler and noise photons satisfies $\eta_c \eta_i \gg \eta_n$. The SNR of quantum memory system is defined as SNR$= \eta_c \eta_i \eta_s / (\eta_c \eta_i \eta_n) = \eta_s / \eta_n$, where $\eta_c \eta_i \eta_n$ means the detected probability of coincidences between idler photons and noise photons. To analyze the contribution of SNR to $g_{s,i}^{(2)}(0)$, SNR is substituted into Eq. (2), then the $g_{s,i}^{(2)}(0)$ can be re-expressed as

$$g_{s,i}^{(2)} \simeq \frac{\eta_s}{\eta_c \eta_s + \eta_n} + 1 = \frac{1}{\eta_c + 1/SNR} + 1. \tag{3}$$

If SNR is large enough, $g_{s,i}^{(2)}(0)$=$1/\eta_c + 1$ will be independent with η_s, which means $g_{s,i}^{(2)}(0)$ will be unaffected by decreasing system storage efficiency once the overall measured efficiency (η_s) of recalled photons is still much larger than that of noise photons (η_n).

Considering the real experimental parameters, the internal generation probability of correlated photon-pairs is 3.54%, and the measured coincidence probability of noise photons and idler photons (i.e., $\eta_c \eta_i \eta_n$) is

0.86×10^{-9} in a 600-ps time window. According to the measured storage efficiency with different storage time, we calculate the SNR with different storage time, as shown in Fig.S. 6(a). The SNR is 730 with storage time up to 230 ns. Besides, we calculate the $g_{s,i}^{(2)}(0)$ with different SNR as shown in the inset of Fig.S. 6(a). It indicates that once the SNR is larger than 20, the $g_{s,i}^{(2)}(0)$ is nearly unaffected. It explains why $g_{s,i}^{(2)}(0)$ keeps unchanged even with longer storage time and decreasing efficiency. According to the measured efficiency, we estimate the $g_{s,i}^{(2)}(0)$ with different storage time, as shown in Fig.S. 6(b), which matches well with the experimental results shown in note 3.

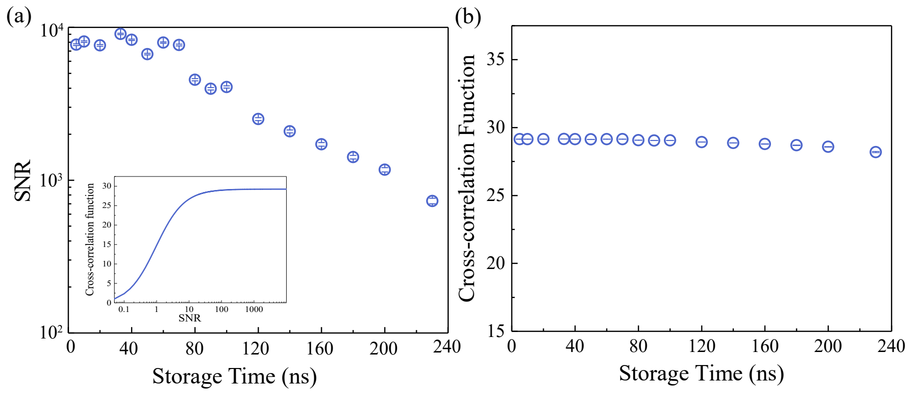

Fig.S. 6: **Cross-correlation function with different SNR.** (a) The SNR of quantum memory versus storage time. Inset: The estimated $g_{s,i}^{(2)}(0)$ versus SNR of quantum memory. (b) The results for the calculation of $g_{s,i}^{(2)}(0)$ with different storage time of quantum memory.

Note 5: Relationship of crosstalk and cross-correlation function

In this section, we describe the relationship of the crosstalk between different channels and the corresponding cross-correlation function $g_{s,i}^{(2)}(0)$. For simplicity, we consider a two-channel quantum memory, shown in Fig.S. 7(a), where 1 and 2 represent the input channels of the quantum memory, $1'$ and $2'$ represent the corresponding outputs of the quantum memory, respectively.

Here we simply consider the crosstalk as the leakage efficiency of photons into the mismatched channels. The crosstalk coefficients of different channels can be expressed as $C_{11'}$, $C_{12'}$, $C_{21'}$, $C_{22'}$ with $C_{ij'}$ $(i, j = 1, 2)$ representing the efficiency of photons from channel i passing through channel j and satisfying $C_{11'}+C_{12'} = 1$, $C_{12'} + C_{22'} = 1$.

As shown in Fig.S. 7(a), here we consider the situation of our experiment. η_i is the overall measured efficiency of idler photons, η_1 is the transmission and collection efficiency of signal photons before quantum memory and η_2 is the measured efficiency of signal photons after the quantum memory, p_1 and p_2 are intrinsic generation efficiency of correlated photon-pairs. According to Eq. (2), the cross-correlation function corresponding to different channels can be expressed as

$$g_{11'} = \frac{p_1\eta_i\eta_1\eta_2 C_{11'} + p_1\eta_i(p_1\eta_1\eta_2 C_{11'} + p_2\eta_1\eta_2 C_{21'})}{p_1\eta_i(p_1\eta_1\eta_2 C_{11'} + p_2\eta_1\eta_2 C_{21'})} = \frac{C_{11'}}{p_1 C_{11'} + p_2 C_{21'}} + 1. \quad (4)$$

$$g_{21'} = \frac{p_1\eta_i\eta_1\eta_2 C_{21'} + p_1\eta_i(p_1\eta_1\eta_2 C_{11'} + p_2\eta_1\eta_2 C_{21'})}{p_1\eta_i(p_1\eta_1\eta_2 C_{11'} + p_2\eta_1\eta_2 C_{21'})} = \frac{C_{21'}}{p_1 C_{11'} + p_2 C_{21'}} + 1. \quad (5)$$

$$g_{12'} = \frac{p_1\eta_i\eta_1\eta_2 C_{12'} + p_1\eta_i(p_1\eta_1\eta_2 C_{12'} + p_2\eta_1\eta_2 C_{22'})}{p_1\eta_i(p_1\eta_1\eta_2 C_{12'} + p_2\eta_1\eta_2 C_{22'})} = \frac{C_{12'}}{p_1 C_{12'} + p_2 C_{22'}} + 1. \quad (6)$$

$$g_{22'} = \frac{p_1\eta_i\eta_1\eta_2 C_{22'} + p_1\eta_i(p_1\eta_1\eta_2 C_{12'} + p_2\eta_1\eta_2 C_{22'})}{p_1\eta_i(p_1\eta_1\eta_2 C_{12'} + p_2\eta_1\eta_2 C_{22'})} = \frac{C_{22'}}{p_1 C_{12'} + p_2 C_{22'}} + 1. \quad (7)$$

It can be clearly seen that the cross-correlation function between uncorrelated channels (1 and $2'$, 2 and $1'$) will be 1 - caused by accidental coincidences of uncorrelated background - only if no crosstalk exists ($C_{12'}$=0, $C_{21'}$=0), otherwise it will be larger than 1. Here, according to the experimental parameters, we assume $g_{12'}$=1 (i.e., $C_{12'}$=0) and $p_1=p_2=p$=0.0354, then calculate the crosstalk $C_{21'}$ between different channels with different $g_{21'}$. The calculated result is shown in Fig.S. 7(b). It indicates that the crosstalk between different channels increases with the increasing of cross-correlation function, thus cross-correlation function is a good indicator to characterize the crosstalk.

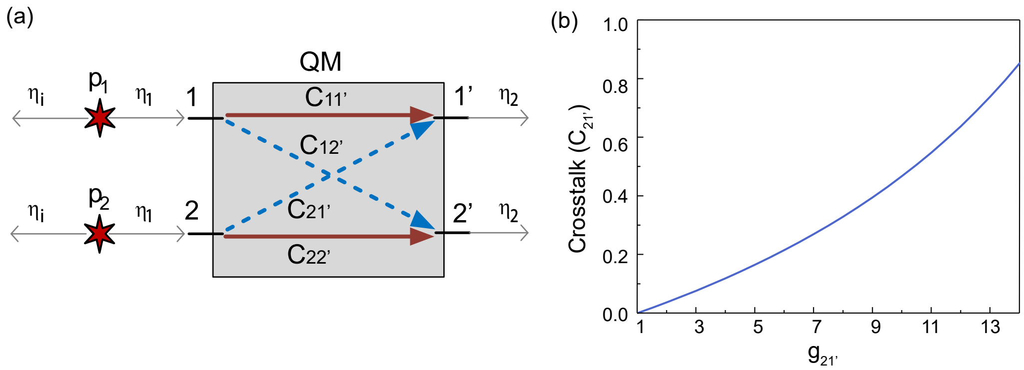

Fig.S. 7: **Relationship of crosstalk and cross-correlation function.** (a) A typical two-channel quantum memory with storage of two pairs of correlated photon-pairs. (b) Crosstalk between two different channels versus cross-correlation function of different channels.

Note 6: The crosstalk of the source and detection system without quantum memory.

The 5×5 array of $g^{(2)}_{s,i}(0)$ between different spectral channels of the photon-pairs source is shown in Fig.S. 8. The results indicate that crosstalk of different spectral channels of the source and detection system is negligible.

Note 7: 1650×1650 array of $g^{(2)}_{s,i}(0)$ between 1650 modes

The total number of spectro-temporal modes is 1650, and the cross-correlation function between 1650 single photon modes is shown in Fig.S. 9(a). (b), (c), (d), and (e) in Fig.S. 9 present parts of $g^{(2)}_{s,i}(0)$ corresponding to different temporal modes retrieved from channel 1, 3, 4, and 5. (modes numbers: 1, 80, 160, 240, 330).

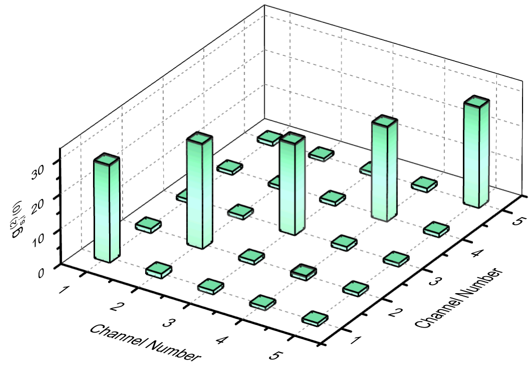

Fig.S. 8: 5 × 5 array of $g^{(2)}_{s,i}(0)$ between different frequency channels of the photon-pairs source. All error bars are calculated by standard deviations of counts which obey Poisson distribution.

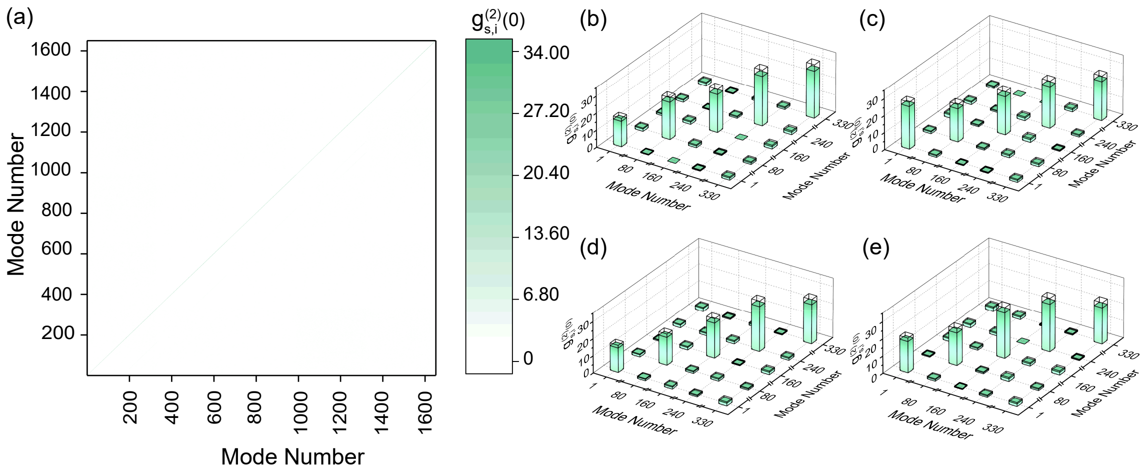

Fig.S. 9: (a) 1650×1650 array of $g^{(2)}_{s,i}(0)$ between 1650 modes. (b), (c), (d), (e) Parts of results of crosstalk measurement among different temporal modes retrieved from channel 1, 3, 4, 5. All error bars are calculated by standard deviations of counts which obey Poisson distribution.

Note 8: Selection of the waiting time before storing signal photons

In order to ensure that recalled photons are not infected by spontaneously emitted photons after spectral tailoring, we measure the counts of spontaneously emitted photons in 1-ns-wide time window versus waiting time. The measuring results are shown in Fig.S. 10. According to the measured results, the waiting time is set to 200 ms.

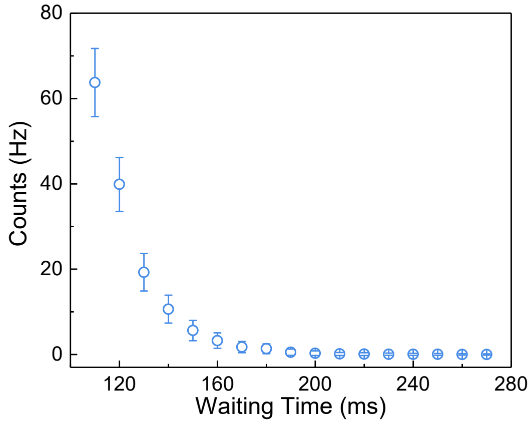

Fig.S. 10: Counts of spontaneously emitted photons in 1-ns-wide time window versus waiting time. All error bars are calculated by standard deviations of counts which obey Poisson distribution.

1. Saglamyurek, E. *et al.* Quantum storage of entangled telecom-wavelength photons in an erbium-doped optical fibre. *Nature Photonics* **9**, 83–87 (2015).
2. Askarani, M. F. *et al.* Entanglement and nonlocality between disparate solid-state quantum memories mediated by photons. *Physical Review Research* **2**, 013039 (2020).
3. Saglamyurek, E. *et al.* A multiplexed light-matter interface for fibre-based quantum networks. *Nature Communications* **7**, 11202 (2016).
4. Wu, R., Supradeepa, V., Long, C. M., Leaird, D. E. & Weiner, A. M. Generation of very flat optical frequency combs from continuous-wave lasers using cascaded intensity and phase modulators driven by tailored radio frequency waveforms. *Optics Letters* **35**, 3234–3236 (2010).
5. Dou, Y., Zhang, H. & Yao, M. Improvement of flatness of optical frequency comb based on nonlinear effect of intensity modulator. *Optics Letters* **36**, 2749–2751 (2011).
6. Arahira, S., Namekata, N., Kishimoto, T. & Inoue, S. Experimental studies in generation of high-purity photon-pairs using cascaded χ (2) processes in a periodically poled linbo 3 ridge-waveguide device. *Journal of The Optical Society of America B-Optical Physics* **29**, 434–442 (2012).
7. Arahira, S., Namekata, N., Kishimoto, T., Yaegashi, H. & Inoue, S. Generation of polarization entangled photon pairs at telecommunication wavelength using cascaded χ (2) processes in a periodically poled linbo 3 ridge waveguide. *Optics Express* **19**, 16032–16043 (2011).
8. Hunault, M., Takesue, H., Tadanaga, O., Nishida, Y. & Asobe, M. Generation of time-bin entangled photon pairs by cascaded second-order nonlinearity in a single periodically poled linbo 3 waveguide. *Optics Letters* **35**, 1239–1241 (2010).
9. Zhang, Z. *et al.* High-performance quantum entanglement generation via cascaded second-order nonlinear processes. *npj Quantum Information* **7**, 123 (2021).
10. Yu, H. *et al.* Spectrally multiplexed indistinguishable single-photon generation at telecom-band. *Photonics Research* **10**, 1417–1429 (2022).
11. De Riedmatten, H., Afzelius, M., Staudt, M. U., Simon, C. & Gisin, N. A solid-state light–matter interface at the single-photon level. *Nature* **456**, 773–777 (2008).
12. Staudt, M. U. *et al.* Investigations of optical coherence properties in an erbium-doped silicate fiber for quantum state storage. *Optics Communications* **266**, 720–726 (2006).
13. De Riedmatten, H. *et al.* Direct measurement of decoherence for entanglement between a photon and stored atomic excitation. *Physical Review Letters* **97**, 113603 (2006).